The Astrophysical Journal, 677:895–905, 2008 April 20

NUCLEAR/CIRCUMNUCLEAR STARBURSTS AND ACTIVE GALACTIC NUCLEUS MASS ACCRETION IN SEYFERT GALAXIES

Yasuyuki Watabe,[1,2,3] Nozomu Kawakatu,[4] and Masatoshi Imanishi[4]
Received 2007 October 16; accepted 2007 December 21

ABSTRACT

We investigated the correlation between nuclear/circumnuclear starbursts around active galactic nuclei (AGNs) and the AGN activities for 43 Seyfert galaxies in the CfA and 12 μm samples. We found that the circumnuclear starburst luminosity, as well as the nuclear starburst luminosity, is positively correlated with the AGN luminosity. Moreover, the nuclear starburst luminosity is more strongly correlated with the AGN luminosity normalized with the AGN Eddington luminosity than is the circumnuclear starburst luminosity. This implies that starbursts nearer the AGN could have a greater effect on AGN mass accretion. We also discuss these results from the viewpoint of the radiation effects from starbursts and sequential starbursts.

Subject headings: galaxies: active — galaxies: nuclei — galaxies: Seyfert — galaxies: starburst — infrared: galaxies

1. INTRODUCTION

Since the discovery of active galactic nuclei (AGNs), the physical mechanism of AGN fueling has remained unresolved. Various fueling mechanisms have been considered thus far; for example, tidal torque driven by a major/minor galaxy merger (Hernquist 1989; Barnes & Hernquist 1991; Mihos & Hernquist 1996; Taniguchi 1999; Saitoh & Wada 2004), tidal torque from nonaxisymmetric gravitational potential due to a stellar bar (Noguchi 1988; Shlosman et al. 1990; Barnes & Hernquist 1992; Knapen et al. 1995; Benedict et al. 1996; Fukuda et al. 2000), a shock or turbulence in the interstellar medium (Fukuda et al. 1998; Montenegro et al. 1999; Wada & Norman 1999, 2001; Maciejewski et al. 2002; Wada et al. 2002; Onodera et al. 2004), and radiation drag from a starburst (Umemura et al. 1997; Fukue et al. 1997; Umemura et al. 1998; Ohsuga et al. 1999).

Numerous observations have gradually clarified circumnuclear starburst events (which are several hundred parsecs to a few kiloparsecs from the center) around AGNs. These starbursts often exhibit patchy and ringlike structures (Pogge 1989; Wilson et al. 1991; Forbes et al. 1994; Marconi et al. 1994; Mauder et al. 1994; Buta et al. 1995; Barth et al. 1995; Leitherer et al. 1996; Maoz et al. 1996; Storchi-Bergmann et al. 1996; Elmouttie et al. 1998; Knapen et al. 2002; Knapen 2005). In addition, hidden nuclear starbursts (within a few hundred parsecs from the center) are found both in Seyfert 1 and 2 galaxies (Imanishi 2002, 2003; Rodríguez-Ardila & Viegas 2003), and the nuclear starburst luminosity is positively correlated with the AGN power (Imanishi & Wada 2004).

These starburst events could strongly influence the structure and the dynamics of gas through the energy input of multiple supernova explosions (Shapiro & Field 1976; Tomisaka & Ikeuchi 1986; Norman & Ikeuchi 1989; Wada & Norman 2002) and the effects of strong radiation (Umemura et al. 1997, 1998; Ohsuga & Umemura 1999, 2001; Kawakatu & Umemura 2002; Watabe & Umemura 2005; Thompson et al. 2005). In particular, for the AGN mass accretion, Wada & Norman (2002) show the possibility of AGN fueling from the effect of chaotic disturbance by the nuclear starburst, using a three-dimensional hydrodynamic simulation. Moreover, Umemura et al. (1997, 1998) have shown that the radiation effects of a circumnuclear starburst could cause AGN fueling.

These theoretical and observational results suggest that some connections exist between nuclear/circumnuclear starbursts and AGN activity. Although a relationship between nuclear starbursts and AGNs has been reported (Imanishi & Wada 2004; Davies et al. 2007), this remains uncertain regarding circumnuclear starbursts. Moreover, it is not clear whether a specific relationship exists between AGN mass accretion and starbursts at various scales. In this study, we investigated the relationship between nuclear/circumnuclear starbursts and AGN activity by considering both nuclear and circumnuclear starbursts.

To investigate the nuclear/circumnuclear starbursts, we used the polycyclic aromatic hydrocarbon (PAH) emission features at 3.3, 6.2, 7.7, and 11.3 μm. The PAHs are excited by far-UV photons, and strong PAH emissions are seen in star-forming regions, whereas a pure AGN shows only a featureless spectrum with virtually no PAH emission. Also, since the dust extinction is much lower for these 3.3–11.3 μm PAH emissions ($\lesssim 0.06 A_V$; Rieke & Lebofsky 1985; Lutz et al. 1996), we can quantitatively estimate modestly obscured ($A_V < 15$ mag) star formation activity by using these emission lines. Throughout this paper, we have adopted $H_0 = 80$ km s^{-1} Mpc^{-1}, $\Omega_M = 0.3$, and $\Omega_\Lambda = 0.7$.

2. SAMPLE DATA

We studied 21 Seyfert 1 galaxies and 22 Seyfert 2 galaxies in the CfA (Huchra & Burg 1992) and 12 μm (Rush et al. 1993) samples, selected on the basis of their host galaxy magnitudes and *IRAS* 12 μm fluxes, respectively. These samples are not expected to be biased toward or against the presence of nuclear starbursts. Our sample was selected from the Imanishi & Wada (2004) data set with both the 3.3 μm PAH luminosity and the nuclear *N*-band luminosity. In their sample, Seyfert galaxies at $z = 0.008$–0.035 were selected such that the nuclear starbursts could be investigated by ground-based spectroscopy, using a 1″–2″ slit,

[1] Center for Computational Sciences, University of Tsukuba, Ten-nodai, 1-1-1 Tsukuba, Ibaraki 305-8577, Japan; watabe@ccs.tsukuba.ac.jp.
[2] INAF–Osservatorio Astrofisico di Arcetri, Largo Enrico Fermi 5, 50125 Firenze, Italy.
[3] Research Fellow of the Japan Society for the Promotion of Science (JSPS).
[4] National Astronomical Observatory of Japan, 2-21-1 Osawa, Mitaka, Tokyo 181-8588, Japan.

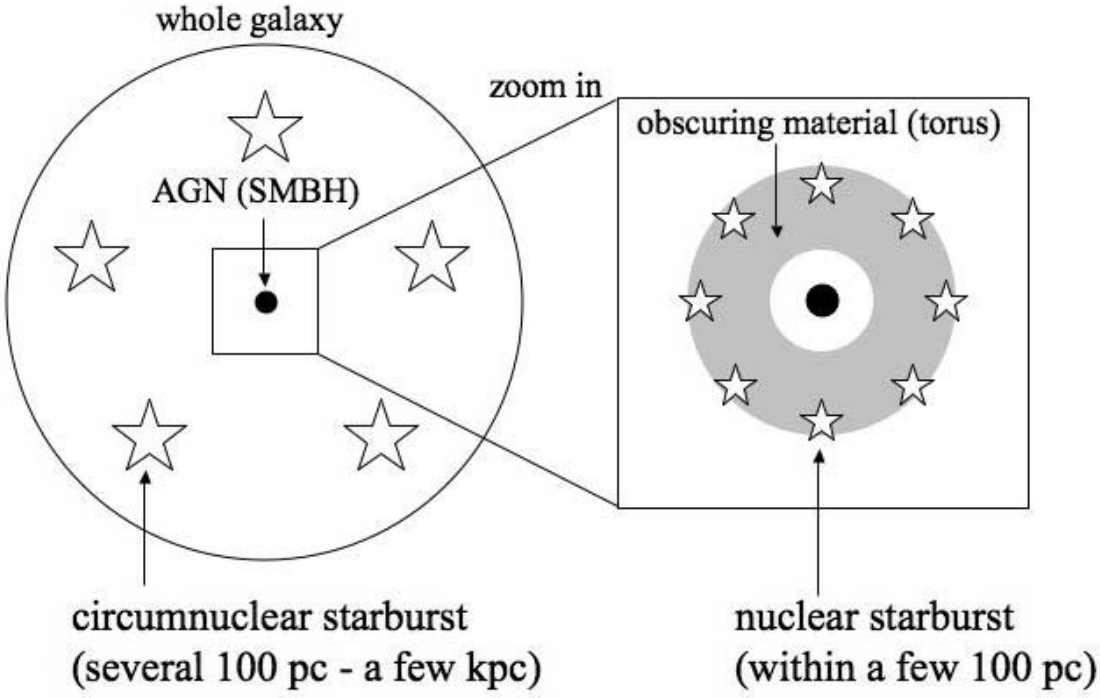

FIG. 1.—Schematic view of the nuclear and circumnuclear starbursts. The nuclear starburst (within a few hundred parsecs) and the circumnuclear starburst (from several hundred parsecs to a few kiloparsecs) are distributed around an AGN.

where $1''$ corresponds to a physical scale of 150 pc ($z = 0.008$) to 650 pc ($z = 0.035$). Also, in order for them to be best observable from Mauna Kea, Hawaii, the declinations of these Seyfert galaxies are limited to being larger than -30°. Due to the telescope limit of the Infrared Telescope Facility (IRTF) 3 m telescope, a restriction of having a declination of less than 68° is also applied. For the Imanishi & Wada (2004) sample, there are no obvious biases.

Among these 43 Seyfert galaxies, we estimated the supermassive black hole (SMBH) mass in order to investigate the mass accretion rate normalized with the AGN Eddington mass accretion rate for 25 objects. In addition to these objects, we estimated the 6.2, 7.7, and 11.3 μm PAH emission for 13 more objects. Also, we collected the X-ray luminosity from data in the literature for 15 objects. Since our sample included some upper limit data, we used statistical techniques that are applicable to a sample in which upper limit data are present.

We focused on both nuclear starbursts, which exist within a few hundred parsecs from the center, and circumnuclear starbursts in the entire host galaxy region. Figure 1 shows a schematic view of the nuclear and circumnuclear starbursts. We can consider the 3.3 μm PAH emission, which was derived through ground-based spectroscopy using the narrow slit, as representing a nuclear starburst. Also, since a circumnuclear starburst is typically much higher than a nuclear starburst (see § 4.2), the 6.2, 7.7, and 11.3 μm PAH emissions, which were observed in the entire host galaxy region, represent a circumnuclear starburst. We describe these processes in detail in §§ 3.1 and 3.2.

3. ESTIMATION OF PHYSICAL PROPERTIES

3.1. *Nuclear Starbursts*

PAH molecules near an AGN can be destroyed by strong X-ray radiation from the AGN (Voit 1992; Siebenmorgen et al. 2004). However, if the PAH molecules are sufficiently shielded by a substantial column density of X-ray–absorbing gas, PAHs can survive even if they are near the AGN. In fact, ample gas is believed to exist that could be related to the obscuring material (the dusty torus in the context of the AGN unified model) around the AGN. In addition, the gravitational stability parameter Q (Toomre 1964) decreases with the radius of the obscuring material, whose mass is notably smaller than that of a SMBH (Imanishi 2003). The gravitational collapse of molecular gas can therefore occur more easily in the outer part of the obscuring material. Thus, in the outer part of the obscuring material, a starburst could take place near the AGN and PAHs could survive there. In fact, from the estimation of the surface brightness values of the 3.3 μm PAH emission (Imanishi & Alonso-Herrero 2004; Imanishi & Wada 2004), which were derived through ground-based spectroscopy using a $1''$–$2''$ slit, this emission should come from nuclear starbursts in the gas-rich region, which may be the obscuring material around AGNs.

Therefore, we can use the 3.3 μm PAH emission data from Imanishi & Alonso-Herrero (2004) and Imanishi & Wada (2004), which were observed with ground-based spectroscopy using the narrow slit, as the indicators of nuclear starbursts. Although any circumnuclear starbursts, which often exhibit ringlike structures with a radius that is of order kiloparsecs from the center, along the slit direction could be also included, the fraction of the circumnuclear starburst emission inside this thin slit is negligible compared to the whole. Thus, the 3.3 μm PAH emission can be regarded as a practical probe for nuclear starbursts in both Seyfert 1 and Seyfert 2 galaxies.

In Imanishi (2003) and Imanishi & Wada (2004), only upper limits for the nuclear 3.3 μm PAH fluxes are available for more than half of the observed Seyfert galaxies. In addition, the observed Seyfert galaxies do not comprise a complete sample. To increase both the number and the fraction of Seyfert galaxies that have detectable nuclear 3.3 μm PAH emission, we newly observed eight additional sources, which are listed in Table 1. Among them,

TABLE 1
Observing Log

Object (1)	Date (UT) (2)	Telescope Instrument (3)	Integration (minutes) (4)	P.A. (deg) (5)	Standard Stars				Remarks (10)
					Name (6)	L (mag) (7)	Type (8)	$T_{\rm eff}$ (K) (9)	
NGC 931 (Mrk 1040)	2007 Aug 26	IRTF SpeX	96	0	HR 720	4.4	G0 V	5930	12 μm Sy1
F03450+0055	2007 Aug 28	IRTF SpeX	112	0	HR 962	3.7	F8 V	6000	12 μm Sy1
NGC 262	2007 Aug 31	IRTF SpeX	80	0	HR 410	5.0	F7 V	6240	12 μm Sy2
NGC 513	2007 Aug 27	IRTF SpeX	120	0	HR 410	5.0	F7 V	6240	12 μm Sy2
MCG −2-8-39	2007 Aug 30	IRTF SpeX	136	0	HR 784	4.5	F6 V	6400	12 μm Sy2
MCG −3-58-7	2007 Aug 30	IRTF SpeX	80	0	HR 8457	4.8	F6 V	6400	12 μm Sy2
Mrk 993	2007 Aug 31	IRTF SpeX	112	0	HR 410	5.0	F7 V	6240	CfA Sy2
0152+06 (UGC 1395)	2007 Aug 29	IRTF SpeX	120	0	HR 508	4.7	G3 V	5800	CfA Sy2

Note.— Col. (1): Object name. Col. (2): Observing date, in UT. Col. (3): Telescope and instrument. Col. (4): Net on-source integration time, in units of minutes. Col. (5): Position angle of the slit, where 0° corresponds to the north-south direction. Col. (6): Standard star name. Col. (7): Adopted L-band magnitude. Col. (8): Stellar spectral type. Col. (9): Effective temperature. Col. (10): Seyfert 1 or 2 galaxy in the 12 μm or CfA sample.

six sources (NGC 931, F03450+0055, NGC 262, NGC 513, MCG −3-58-7, and Mrk 993) showed possible signs of the 3.3 μm PAH emission in our previously obtained infrared 3–4 μm spectra (Imanishi 2003; Imanishi & Wada 2004). Therefore, we decided to reobserve these sources with longer exposures to check whether the signs were real or not. The two other sources (MCG −2-8-39 and 0152+06) were newly observed this time in order to increase the number of observed sources. We include the details of these observations in the Appendix.

3.2. *Circumnuclear Starbursts*

To estimate the absolute magnitudes of circumnuclear starburst activity in Seyfert galaxies, we analyzed archival infrared data obtained with the Infrared Spectrograph (IRS; Houck et al. 2004) on board the *Spitzer Space Telescope* (Werner et al. 2004) through program 3269 (PI: J. Gallimore). We focused on the infrared spectra of Short-Low 2 (SL2; 5.2–7.7 μm) and Short-Low 1 (SL1; 7.4–14.5 μm), in order to estimate the fluxes of PAH emission features at $\lambda_{\rm rest} = 6.2$, 7.7, and 11.3 μm in the rest frame.

We used the latest pipeline-processed data products at the time of our analysis (ver. S11–14, post-BCD files). The observations were performed with the slit-scan mode, and the entire host galaxy regions of the Seyfert galaxies were covered. We summed all the signals and extracted the spectra after subtracting the background emission in a standard manner. Thus, the resulting spectra should reflect the emission from the entire regions of the Seyfert galaxies. Wavelength and flux calibrations for the SL data were made on the basis of the files `b0_wavsamp.tbl` and `b0_fluxcon.tbl` of the *Spitzer* pipeline-processed data, respectively. For the SL1 spectra, data at $\lambda_{\rm obs} > 14.5$ μm in the observed frame are invalid (Infrared Spectrograph Data Handbook, version 1.0)[5] and so were removed. For some faint sources, appropriate spectral binning was applied to reduce the scatter of data points and to achieve more reliable measurements of the PAH fluxes.

The circumnuclear starburst luminosity is typically much higher than the nuclear starburst luminosity (Imanishi 2003; Imanishi & Wada 2004; see also § 4.2 and Table 2). Thus, we consider the 6.2, 7.7, and 11.3 μm PAH emission, which were observed in the entire host galaxy regions, to be good indicators of a circumnuclear starburst even if these PAH luminosities contain a small contribution from nuclear starbursts.

[5] Available at http://ssc.spitzer.caltech.edu/irs/dh/.

3.3. *AGN Luminosity*

In order to measure AGN activity, we used the nuclear N-band (10.5 μm) luminosity measured with a 1.5″ aperture (Gorjian et al. 2004), since the contribution of starbursts for the nuclear N-band luminosity is small (Gorjian et al. 2004). However, the nuclear N-band luminosity represents the reemission of hot dust illuminated by the AGN. Thus, it may contain some uncertainties due to the dust distribution and the covering factor of the dusty torus around the AGN. To examine whether the nuclear N-band luminosity represents AGN activity in the sample data, we also considered the absorption-corrected hard (2–10 keV) X-ray luminosity, which is regarded as the AGN intrinsic luminosity for the Compton-thin AGNs, by using data from the literature (see references in Table 3).

3.4. *Black Hole Mass*

Next we estimated the SMBH mass, $M_{\rm BH}$, in order to investigate the mass accretion rate normalized with the AGN Eddington mass accretion rate. In order to estimate the SMBH masses of Seyfert 1 galaxies, we used the following method (for details, see Kawakatu et al. 2007). The method for estimating the mass of a SMBH is based on the assumptions that the motion of ionized gas clouds moving around the SMBH is dominated by the gravitational force and that the clouds within the broad-line region

TABLE 2
Properties of the Nuclear 3.3 μm PAH Emission Feature

Object (1)	Flux ($\times 10^{-14}$ ergs s^{-1} cm^{-2}) (2)	Luminosity ($\times 10^{40}$ ergs s^{-1}) (3)	Rest EW$_{3.3\rm PAH}$ (nm) (4)
NGC 931	<6.5	<2.9	<2.5
F03450+0055	1.8	3.1	1.0
NGC 262	<3.3	<1.3	<1.6
NGC 513	0.5	0.3	3.5
MCG −2-8-39	<1.3	<2.0	<13
MCG −3-58-7	1.8	3.3	1.1
Mrk 993	<2.2	<0.9	<16
0152+06	<1.6	<0.8	<13

Note.—Col. (1): Object name. Col. (2): Observed nuclear 3.3 μm PAH flux. Col. (3): Observed nuclear 3.3 μm PAH luminosity. Col. (4): Rest-frame equivalent width of the 3.3 μm PAH emission.

TABLE 3

DATA FROM SEYFERT GALAXIES

Object (1)	z (2)	$\log L_{3.3}$ ($L_\odot$) (3)	$\log L_{6.2}$ ($L_\odot$) (4)	$\log L_{7.7}$ ($L_\odot$) (5)	$\log L_{11.3}$ ($L_\odot$) (6)	$\log L_{N1.5''}$ ($L_\odot$) (7)	$\log M_{BH}$ ($M_\odot$) (8)	$\log E_N$ (9)	$\log L_X$ ($L_\odot$) (10)	References (11)
Seyfert 1 (CfA Sample)										
Mrk 335	0.025	6.85	?	?	?	10.06	6.89	−1.34	9.43	1
NGC 863 (Mrk 590)	0.027	<6.88	...	...	...	...	7.58	...	9.95	2
NGC 3786 (Mrk 744)	0.009	<6.36	...	...	...	...	7.53	...	...	
NGC 4235	0.008	6.00	...	...	...	...	...	...	8.58	3
NGC 4253 (Mrk 766)	0.013	6.67	...	...	...	9.71	6.54	−1.34	9.09	1
NGC 5548	0.017	<6.76	...	...	...	10.01	7.92	−2.42	9.77	1
Mrk 817	0.031	7.36	8.41	8.7	8.2	10.43	7.72	−1.80	...	
NGC 7469	0.016	<6.9	8.93	9.27	8.88	9.99	7.52	−2.04	9.61	1
Mrk 530 (NGC 7603)	0.029	7.24	8.56	8.64	8.48	10.01	...	...	...	
Seyfert 1 (12 μm Sample)										
NGC 931 (Mrk 1040)	0.016	<6.88[a]	<7.47	<8.22	7.87	9.82	7.13	−1.82	8.76	1
F03450+0055	0.031	6.91[a]	?	?	?	10.07	...	...	...	
3C 120	0.033	7.4	...	...	...	10.17	7.41	−1.76	10.38	2
Mrk 618	0.035	7.21	...	...	...	<9.95	...	...	...	
MCG −5-13-17	0.013	<6.56	...	...	...	9.46	...	...	...	
Mrk 79	0.022	<7.03	?	?	?	10.15	7.68	−2.05	...	
Mrk 704	0.030	<6.95	...	...	...	10.52	...	...	...	
NGC 2992	0.008	<6.44	...	...	...	9.10	...	...	9.30	2
Mrk 1239	0.019	<6.31	...	...	...	10.11	6.62	−1.02	...	
MCG −2-33-34	0.014	6.53	...	...	...	<8.86	...	...	...	
IC 4329A	0.016	<7.25	?	?	?	10.46	6.64	−0.69	9.95	1
Mrk 509	0.036	7.36	...	...	...	10.48	7.83	−1.86	...	
Seyfert 2 (CfA Sample)										
NGC 4388	0.008	<6.03	7.68	8.17	7.73	9.24	7.22	−2.49	8.08	3
NGC 5252	0.023	<7.11	...	...	...	...	...	...	9.23	4
NGC 5256 (Mrk 266SW)	0.028	7.48	8.96	9.30	8.84	9.83	>6.92	<−1.60	...	
NGC 5347	0.008	<6.26	<7.05	<7.45	<7.02	9.22	6.79	−2.08	...	
NGC 5929	0.008	<5.59	<6.78	<7.32	<6.64	<8.37	7.25	<−3.39	...	
NGC 7674	0.029	7.49	8.30	9.03	8.58	10.41	7.56	−1.66	...	
Seyfert 2 (12 μm Sample)										
Mrk 938	0.019	7.82	...	...	...	9.85	...	...	...	
NGC 262 (Mrk 348)	0.015	<6.53[a]	<7.11	?	<7.29	9.52	7.21	−2.20	8.91	5
NGC 513	0.020	5.89[a]	8.45	8.73	8.43	<9.69	7.65	<−2.47	...	
NGC 1125	0.011	6.74	...	...	...	<8.95	...	...	...	
NGC 1241	0.014	<5.97	<7.53	<7.63	<7.23	<9.38	7.46	<−2.59	...	
NGC 1320 (Mrk 607)	0.010	6.44	...	...	...	9.45	7.18	−2.24	...	
F04385−0820	0.015	6.61	...	...	...	9.64	...	...	...	
NGC 1667	0.015	<6.21	8.7	9.05	8.65	<9.46	7.88	<−2.93	...	
NGC 3660	0.012	6.4	...	...	...	<9.29	...	...	...	
NGC 4968	0.010	6.59	...	...	...	9.49	...	...	...	
MCG −3-34-64	0.017	<6.61	...	...	...	10.32	...	...	...	
NGC 5135	0.014	7.12	...	...	...	9.46	7.35	−2.40	...	
MCG −2-40-4 (NGC 5995)	0.024	<7.26	...	...	...	10.19	...	...	9.88	5
F15480−0344	0.030	<7.13	...	...	...	10.04	...	...	...	
NGC 7172	0.009	<6.28	...	...	...	9.04	7.67	−3.14	9.29	2
MCG −3-58-7	0.032	<7.25	...	...	...	10.40	...	...	...	

NOTES.—Col. (1): Object name. Col. (2): Redshift. Cols. (3)–(6): PAH luminosity at 3.3, 6.2, 7.7, and 11.3 μm, respectively. Col. (7): PAH luminosity at the nuclear N band (10.5 μm). Col. (8): Black hole mass. Col. (9): Ratio of nuclear N-band luminosity to AGN Eddington luminosity. Cols. (10) and (11): Absorption-corrected hard (2–10 keV) X-ray luminosity, and corresponding references. Ellipses indicate that no information was available. Question marks indicate undetected PAH emission.

[a] Taken from this paper.

REFERENCES.—(1) O'Neill et al. 2005; (2) Shinozaki et al. 2006; (3) Panessa et al. 2006; (4) Turner et al. 1997; (5) Panessa & Bassani 2002.

(BLR) are virialized (e.g., Peterson & Wandel 1999). By adopting an empirical relationship (Kaspi et al. 2000) between the size of the BLR and the rest-frame optical continuum luminosity, $\lambda L_{\lambda}(5000\ \text{Å})$ and reverberation mapping, we can obtain the following formula:

$$M_{\rm BH} = 4.9^{+0.4}_{-0.3} \times 10^6 \left[\frac{\lambda L_{\lambda}(5100\ \text{Å})}{10^{44}\ \text{ergs s}^{-1}}\right]^{0.70\pm0.033} \times \left(\frac{v_{\rm FWHM}}{10^3\ \text{km s}^{-1}}\right)^2 M_{\odot}. \quad (1)$$

We can use this equation to estimate the masses of SMBHs in Seyfert 1 galaxies.

We cannot use the above method for Seyfert 2 galaxies because no broad emission components exist for these galaxies. So we used the data of the SMBH mass (Bian & Gu 2007), which is estimated from the relation between the SMBH mass and the stellar velocity dispersion, σ_* (Tremaine et al. 2002):

$$M_{\rm BH} = 10^{8.13}\left(\frac{\sigma_*}{200\ \text{km s}^{-1}}\right)^{4.02} M_{\odot}. \quad (2)$$

4. RESULTS

4.1. *Nuclear* 3.3 μm *PAH Emission*

Figure 2 represents the zoom-in spectra around the 3.3 μm PAH emission feature of the observed Seyfert galaxies. Thanks to the excellent observing conditions and longer exposures, the flux excesses at the expected wavelength of the 3.3 μm PAH emission feature at $3.3(1+z)$ μm are now recognizable in three sources (F03450+0055, NGC 513, and MCG −3-58-7), marked with "3.3 μm PAH" in Figure 2. For these sources, the fluxes, luminosities, and rest-frame equivalent widths ($\text{EW}_{3.3\text{PAH}}$) of the 3.3 μm PAH emission were estimated using Gaussian fits. For the remaining five sources, which have no clear 3.3 μm PAH detection [marked with "3.3 μm PAH (?)" in Fig. 2], we estimated the upper limits of the PAH strengths by adopting the lowest plausible continuum levels and assuming the profile of type 1 sources in Tokunaga et al. (1991) as a 3.3 μm PAH template. Table 2 summarizes the results.

At $\lambda_{\rm rest} \sim 3.3$ μm in the rest frame, Pfδ (3.30 μm) emission is present, superposed on the 3.3 μm PAH emission. The relative contribution from this Pfδ emission line is expected to be high in Seyfert 1 galaxies, because broad emission line components are unobscured. However, the equivalent width of the Pfδ line is expected to be ∼0.3 nm for a typical Seyfert 1 galaxy (Imanishi et al. 2006), and even lower in a Seyfert 2 galaxy. This equivalent width value is much lower than the observed values or upper limits in Table 2. We thus ascribe the flux excess at $\lambda_{\rm rest} = 3.3$ μm mostly to the 3.3 μm PAH emission feature.

Among the six previously observed Seyfert galaxies, the detected 3.3 μm PAH fluxes or their upper limits are lower than previously derived upper limits (Imanishi 2003; Imanishi & Wada 2004), except for those of NGC 931. For NGC 931, our new upper limit of the 3.3 μm PAH flux is ∼50% higher than our previous estimate (Imanishi & Wada 2004), possibly because our new estimate is a conservative one, derived on the basis of the lowest plausible continuum level. The 3–4 μm continuum flux levels are also similar to within ∼50% between the spectra in this paper and those in our previous papers (Imanishi 2003; Imanishi & Wada 2004), except for those of NGC 513. The flux of NGC 513 in this paper is more than 1 mag fainter than that in Imanishi (2003), possibly because of the narrower slit employed and/or the flux variation of the 3–4 μm continuum emission, which originates in AGN-heated hot dust.

4.2. 6.2, 7.7, *and* 11.3 μm *PAH Emission*

Figures 3 and 4 represent the 5.2–14.5 μm spectra of Seyfert 1 and 2 galaxies, respectively. Most of the Seyfert galaxies in Figures 3 and 4 show clearly detectable PAH emission features at $\lambda_{\rm rest} = 6.2$, 7.7, and 11.3 μm.

To estimate the fluxes of the PAH emission features at $\lambda_{\rm rest} =$ 6.2, 7.7, and 11.3 μm, we adopted a linear continuum determined from data points on the shorter and longer wavelength sides of individual PAH features, as was done in Imanishi et al. (2007). The adopted continuum levels are shown as solid straight lines in Figures 3 and 4. We fitted the PAH emission features with Gaussian profiles, which reproduced the observed data reasonably well. We treated the weak (lower than 3 σ) or undetected PAH emission as upper limits or nonflux, respectively.

By using the 3.3, 6.2, and 11.3 μm PAH luminosities, we can roughly estimate the infrared luminosities of the nuclear starburst and the total starburst. In Table 4, we show the infrared luminosities of the nuclear starburst, estimated from the 3.3 μm PAH luminosity, $L_{\rm IR,3.3} = 10^3 L_{3.3}$ (Mouri et al. 1990; Imanishi 2002), and of the total starburst, estimated from the 6.2 and 11.3 μm PAH luminosities as $L_{\rm IR,6.2} = (3\times10^2)L_{6.2}$ (Peeters et al. 2004) and $L_{\rm IR,11.3} = (7\times10^2)L_{11.3}$ (Soifer et al. 2002), respectively. The infrared luminosities of the total starbursts are several times or more larger than those of nuclear starbursts. This means that the circumnuclear starbursts dominate the total starburst luminosity. Thus, we can consider the 6.2, 7.7, and 11.3 μm PAH emissions, which were observed in the entire host galaxy regions, as good indicators of a circumnuclear starburst.

4.3. *Luminosity Correlation between Nuclear/Circumnuclear Starbursts and AGNs*

In Figure 5, we examine a possible correlation between the nuclear *N*-band luminosity and the hard X-ray luminosity. We applied the generalized Kendall rank correlation statistics (Isobe et al. 1986) provided in the Astronomy Survival Analysis package (ASURV; Feigelson & Nelson 1985; Isobe et al. 1986) to both types of Seyfert galaxies. The probability that a correlation is not present was 0.9% (2.6 σ). Since the hard X-ray luminosity is the absorption-corrected luminosity and is estimated for Compton-thin AGNs, this correlation means that the nuclear *N*-band luminosity is a good indicator of AGN activity for these samples of Seyfert galaxies.

In Figure 6, we have plotted the nuclear *N*-band luminosity and the hard X-ray luminosity versus the 3.3 μm PAH emission luminosity. The probability that a correlation is not present was 0.7% (2.7 σ) and 5.3% (1.9 σ) for the nuclear *N*-band luminosity and the hard X-ray luminosity, respectively. Imanishi & Wada (2004) show a positive correlation between the 3.3 μm luminosity and the nuclear *N*-band luminosity. We also obtained the same results for the hard X-ray luminosity. Thus, the correlation between the luminosity of the nuclear starbursts and that of the central AGN is also statistically confirmed in Seyfert galaxies in the hard X-ray luminosity, which is directly involved in AGN activity. These nuclear *N*-band and hard X-ray results definitely show that the nuclear starburst luminosity is positively correlated with the AGN power.

The probability of a correlation between the hard X-ray luminosity and the 3.3 μm PAH luminosity is lower than that between the nuclear *N*-band luminosity and the PAH luminosity. This

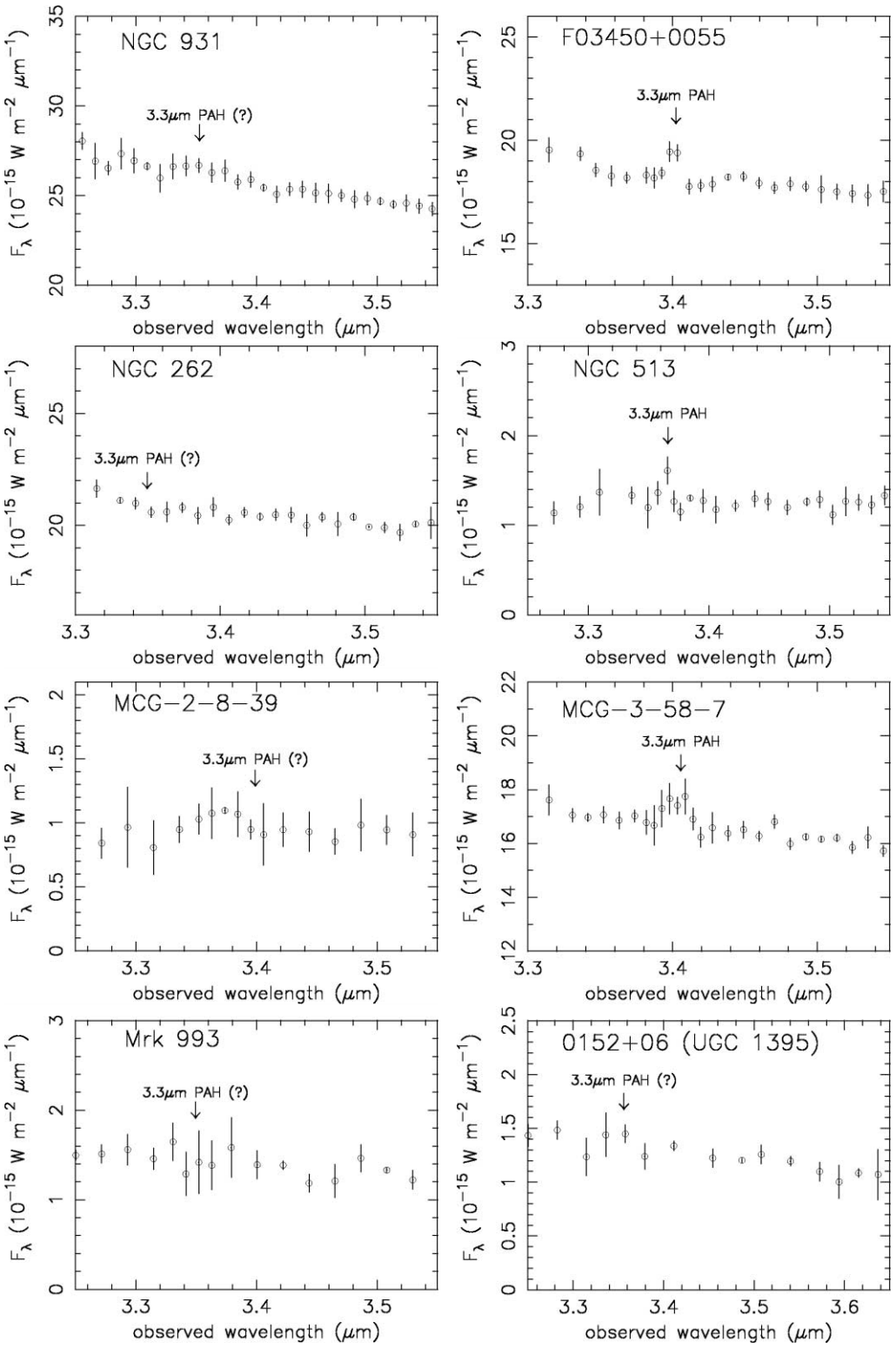

FIG. 2.—Zoom-in spectra around the redshifted 3.3 μm PAH emission feature (*arrows*) of the eight observed Seyfert galaxies. The horizontal and vertical axes indicate the observed wavelength in units of μm and F_λ in units of 10^{-15} W m^{-2} μm^{-1}, respectively.

difference may result from a large number of upper/lower limit data and few sample data. To analyze the hard X-ray data in detail, we may need to eliminate these uncertainties and collect more data. We therefore focus on only the nuclear *N*-band luminosity for the following results.

In Figure 7, we have plotted the nuclear *N*-band luminosity versus the energy for the 6.2, 7.7, and 11.3 μm PAH emissions. Since these PAH emissions cover the entire host galaxy, we can consider them as indicators of circumnuclear starbursts. We also plotted the energy for the 3.3 μm PAH emission in Figure 7 and applied the generalized Kendall rank correlation statistics to the 6.2, 7.7, and 11.3 μm PAH emissions simultaneously. The probability that a correlation is not present was found to be 0.35% (2.9 σ) for these PAH emissions. Thus, not only the nuclear

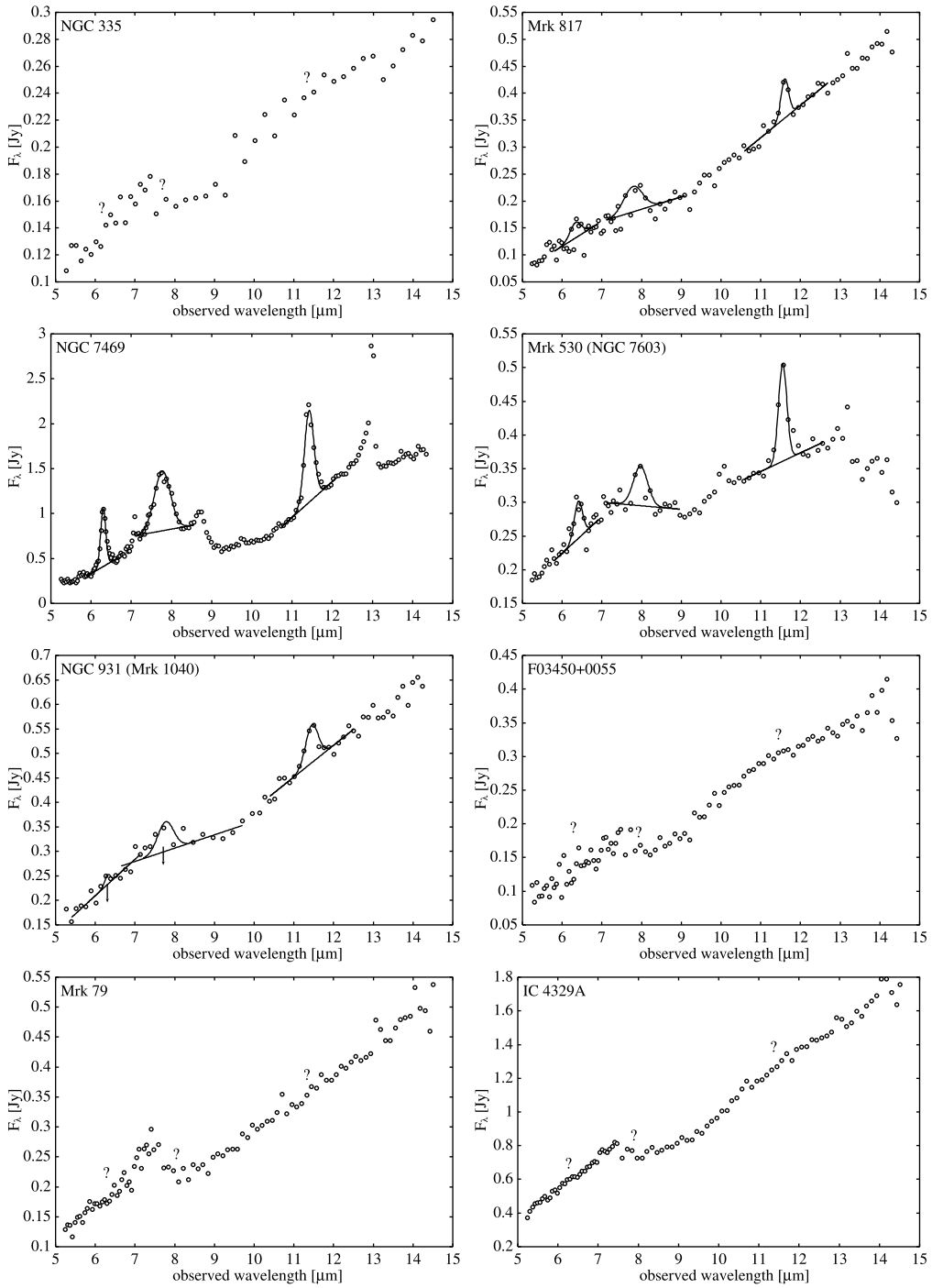

FIG. 3.—Plots of 5.2–14.5 μm spectra of Seyfert 1 galaxies. The horizontal and vertical axes indicate the observed wavelength in units of μm and F_λ in units of Jy, respectively. The solid straight lines represent the adopted continuum with which we estimate each PAH emission flux. The solid curves are Gaussian profile fittings of PAH emission. The arrows and question marks indicate weak (lower than 3 σ) and undetected PAH emission, respectively.

starburst luminosity, but also the circumnuclear starburst luminosity, are connected to the AGN luminosity.

4.4. *AGN Mass Accretion and Star-forming Activity*

In Figure 8, we have also plotted the ratio of the nuclear *N*-band luminosity to the AGN Eddington luminosity, $L_{\mathrm{N1.5''}}/L_{\mathrm{Edd}}$, versus the energy of the nuclear/circumnuclear starbursts. The probability that a correlation is not present was found to be 4.8% (2.0 σ) for the nuclear starbursts (3.3 μm PAH emission) and 16.7% (1.4 σ) for the circumnuclear starbursts (the other PAH emissions). Thus, we statistically confirmed that the nuclear starbursts are also positively correlated with the AGN luminosity normalized with the Eddington luminosity, whereas the circumnuclear starbursts are only weakly correlated.

Here PAH emissions are associated with star formation, and so we can also interpret the horizontal axis as being an indicator of star-forming activity. The vertical axis also represents the mass accretion rate normalized with the Eddington mass accretion rate. This ratio corresponds to the efficiency of gas accretion onto a given SMBH mass. Thus, these results could be interpreted as showing the relationship between the efficiency of gas accretion onto a given SMBH mass and the star-forming activity around the

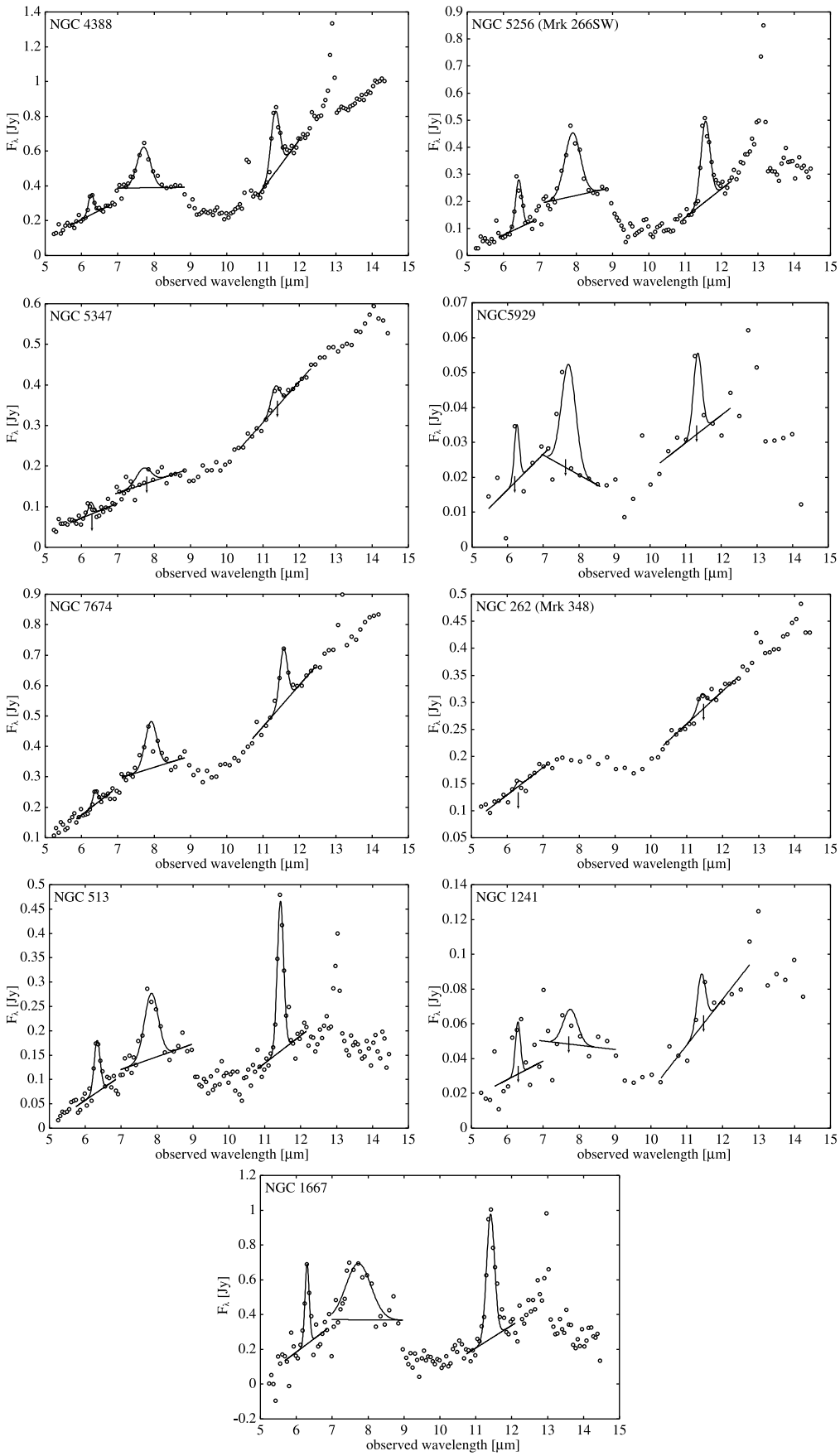

FIG. 4.—Same as Fig. 3, but for Seyfert 2 galaxies.

TABLE 4
INFRARED LUMINOSITY

Object (1)	$\log L_{IR,3.3}$ ($L_\odot$) (2)	$\log L_{IR,6.2}$ ($L_\odot$) (3)	$\log L_{IR,11.3}$ ($L_\odot$) (4)	$L_{IR,6.2}/L_{IR,3.3}$ (5)	$L_{IR,11.3}/L_{IR,3.3}$ (6)
Mrk 817	10.36	10.88	11.05	3.30	4.94
NGC 7469	<9.90	11.40	11.73	>31.52	>68.21
Mrk 530 (NGC 7603)	10.24	11.03	11.33	6.14	12.41
NGC 931 (Mrk 1040)	<9.88	<9.94	10.72	...	>6.98
NGC 4388	<9.03	10.15	10.58	>13.14	>35.80
NGC 5256 (Mrk 266SW)	10.48	11.43	11.69	8.88	16.36
NGC 5347	<9.26	<9.52	<9.87	...	...
NGC 5929	<8.59	<9.25	<9.49	...	...
NGC 7674	10.49	10.77	11.43	1.90	8.79
NGC 262 (Mrk 348)	<9.53	<9.58	<10.14	...	...
NGC 513	8.89	10.92	11.28	106.79	247.67
NGC 1241	<8.97	<10.00	<10.08	...	...
NGC 1667	<9.21	11.17	11.50	>90.89	>196.73

NOTES.—Col. (1): Object name. Col. (2): Infrared luminosity of the nuclear starburst, where $L_{IR,3.3} = 10^3 L_{3.3}$ (Mouri et al. 1990; Imanishi 2002). Cols. (3) and (4): Infrared luminosity of the total starburst, where $L_{IR,6.2} = (3 \times 10^2) L_{6.2}$ (Peeters et al. 2004) and $L_{IR,11.3} = (7 \times 10^2) L_{11.3}$ (Soifer et al. 2002) were estimated from the 6.2 and 11.3 μm PAH luminosity, respectively. Cols. (5) and (6): Infrared luminosity ratios of the total starburst to the nuclear starburst. Ellipses indicate that the infrared luminosities of both the nuclear starburst and the total starburst are upper limit data.

AGN. Our results show a close correlation between the star-forming activity that is closer to the AGN and the efficiency of gas accretion. Therefore, starbursts near the AGN could affect the AGN mass accretion more effectively.

5. DISCUSSION: LINK BETWEEN AGN MASS ACCRETION AND NUCLEAR/CIRCUMNUCLEAR STARBURSTS

We found that nuclear and circumnuclear starburst luminosities are positively correlated with AGN luminosity. However, the nuclear starburst luminosity is more strongly correlated with the AGN mass accretion, compared to the circumnuclear luminosity. These results imply that the AGN mass accretion could be connected to the star formation activity around AGNs. Therefore, here we discuss the interpretation of our results, focusing on the effect of star formation activities.

Umemura et al. (1997, 1998) showed the mass accretion onto galactic nuclei by the radiation effect from a circumnuclear starburst.

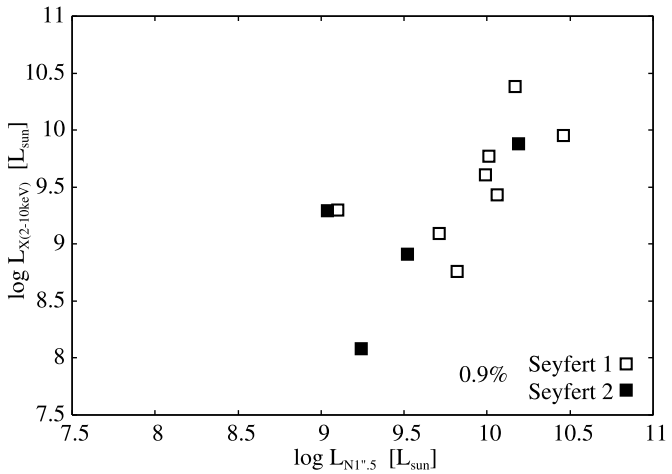

FIG. 5.—Correlation between nuclear *N*-band luminosity and hard X-ray luminosity. The horizontal and vertical axes indicate the nuclear *N*-band luminosity and the absorption-corrected hard (2–10 keV) X-ray luminosity, respectively. The percentage represents the probability that a correlation is not present.

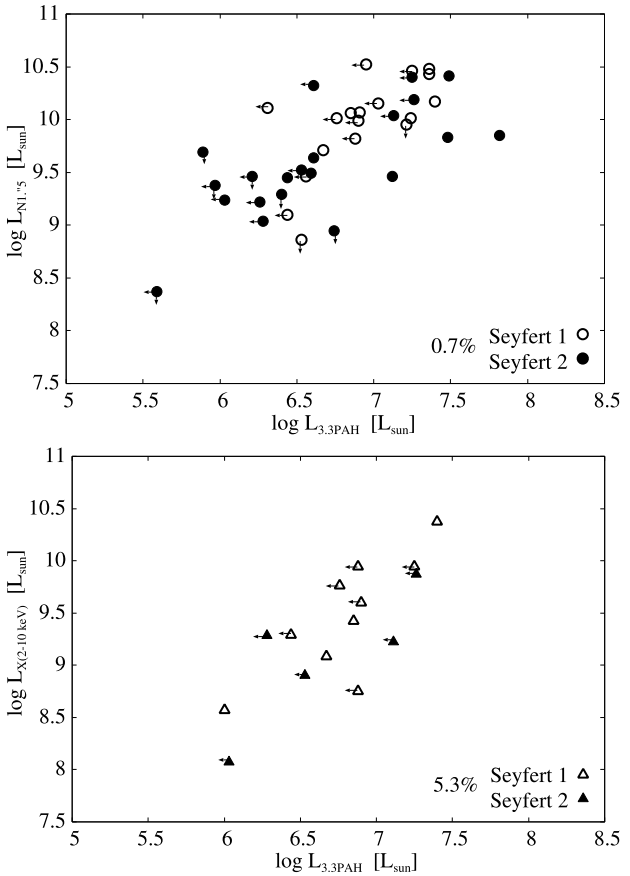

FIG. 6.—Nuclear *N*-band luminosity and hard X-ray luminosity vs. the 3.3 μm PAH emission luminosity. *Top*: The horizontal axis indicates the nuclear 3.3 μm PAH emission luminosity detected inside slit spectra (Imanishi & Wada 2004; this paper). The vertical axis represents the nuclear *N*-band (10.5 μm) luminosity as measured with a ground-based two-dimensional camera with a 1.5″ aperture (Gorjian et al. 2004). *Bottom*: Same as above, but the vertical axis represents the absorption-corrected hard (2–10 keV) X-ray luminosity. The percentage represents the probability that a correlation is not present.

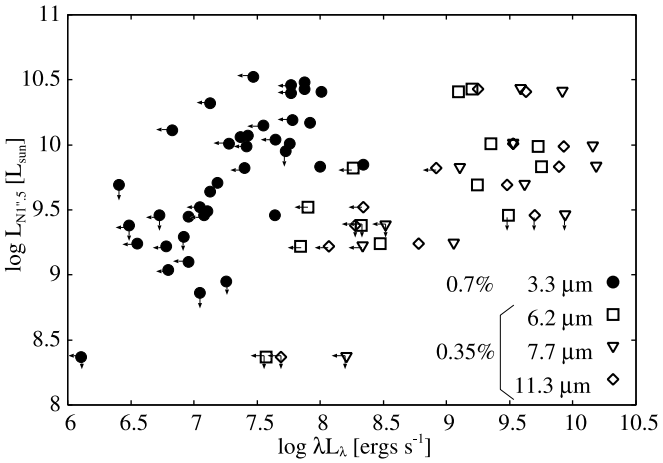

FIG. 7.—Nuclear *N*-band luminosity vs. the energy of nuclear/circumnuclear starbursts. The horizontal axis indicates the energy of the 3.3, 6.2, 7.7, and 11.3 μm PAH emission, and the vertical axis represents the nuclear *N*-band luminosity. The percentages represent the probability that a correlation is not present.

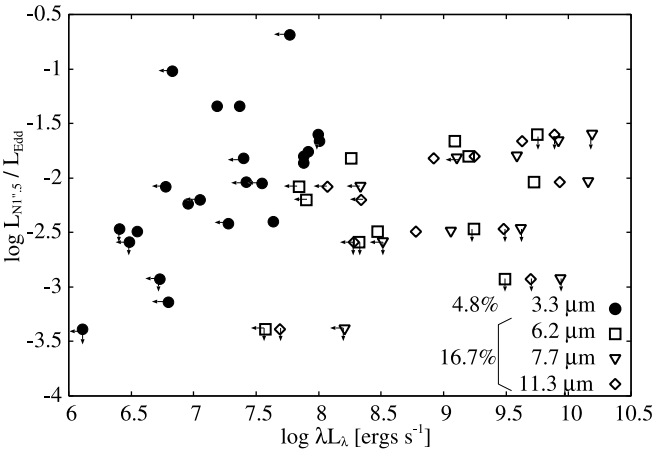

FIG. 8.—Same as Fig. 7, but the vertical axis represents the ratio of the nuclear *N*-band luminosity to the AGN Eddington luminosity.

They assumed a circumnuclear starburst ring and a gas disk within the starburst ring.

Through radial radiation pressure from the circumnuclear starburst, the optically thin surface layer of the gas disk (or the whole of the optically thin disk) is made to contract. Then the surface layer sheds angular momentum because of the radiation drag. Also, since the radiation drag timescale for the dusty gas has been estimated to be a few $\times 10^6$ yr and the radial radiation pressure has more influence at shorter timescales (Umemura et al. 1998), due to these mechanisms, luminous starbursts could carry a larger amount of gas toward the inner region within the duration of the starburst phase, which is 10^7 yr (e.g., Efstathiou et al. 2000), and the typical age for AGNs, which is 10^8 yr (basically the Eddington timescale).

Radial radiation pressure may induce star formation, as well as contraction of the gas disk shock (Umemura et al. 1998). The superbubble driven by sequential explosions of supernovae in an OB association located in the plane-stratified gas distribution may also compress the surrounding gas due to shocks (Shapiro & Field 1976; Tomisaka & Ikeuchi 1986; Norman & Ikeuchi 1989), and new stars may be born there. In fact, Matsushita et al. (2005) showed clear evidence of such a self-induced starburst at the inner edge of the expanding molecular superbubble in M82. This effect is even more expected in the case of a luminous starburst. If star formation is initiated in the contracted gas, it may induce further radiation effects and/or a superbubble in the inner gas disk. If the starbursts occur in such a sequential manner, the gas will be carried farther into the inner region, and sequential starbursts may produce nuclear starbursts with some time lag (e.g., the timescale of the radiation pressure and radiation drag and/or the expansion time of the superbubble).

Also, Fukuda et al. (2000) showed that the gas ring in a barred galaxy could be unstable to gravitational instability and could fragment into gas clumps. These clumps fall to the center due to the torque from the massive clumps and/or the dynamical friction from the stellar component (Makino 1997). Such dynamical effects could be also related to the gas accretion toward the center and could produce nuclear starbursts.

Although the nuclear starbursts are hidden by dusty gas, the structure is expected to be clumpy (Wada & Norman 2002). In this case, not only the chaotic disturbance of the gas, but also the radiation drag from the nuclear starburst, may be able to reduce the angular momentum of the clumpy gas (Kawakatu & Umemura 2002). Therefore, this innermost starburst could be directly related to the AGN mass accretion.

6. CONCLUSION

To determine whether starbursts influence AGN activity, we investigated the correlation between nuclear/circumnuclear starbursts and AGN activity. We found that the circumnuclear starburst luminosity, as well as the nuclear starburst luminosity, is positively correlated with the AGN luminosity. Moreover, nuclear starbursts are also positively correlated with the AGN luminosity normalized with the AGN Eddington luminosity, whereas the circumnuclear starburst is only weakly correlated. This implies that close connections exist between starbursts nearer the AGN and AGN mass accretion.

We thank K. Wada and T. Nagao for providing valuable discussions. We also thank the anonymous referee for valuable comments. Y. W. is supported by the Research Fellowship of the JSPS for Young Scientists. M. I. is supported by Grants-in-Aid for Scientific Research (19740109).

APPENDIX

ZOOM-IN SPECTRA AROUND REDSHIFTED 3.3 μm PAH EMISSION FEATURE

The infrared 3–4 μm spectra of the eight Seyfert galaxies were taken using the IRTF instrument SpeX (Rayner et al. 2003). The 1.9–4.2 μm cross-dispersed mode with a 0.8″ wide slit was employed. This mode enables *L*-band (2.8–4.1 μm) and *K*-band (2–2.5 μm) spectra to be obtained simultaneously, with a spectral resolution of $R \sim 1000$. The sky conditions were photometric throughout the observations, and the seeing at the *K* band was measured to be in the range 0.35″–0.45″ FWHM. A standard telescope nodding technique (ABBA pattern) with a throw of 7.5″ was employed along the slit. The telescope tracking was monitored with the infrared slit-viewer of SpeX. Each exposure was 15 s long, and 2 co-adds were made at each position.

F- or G-type main-sequence stars (Table 1) were observed as standard stars, with a mean air mass difference of <0.1 to the individual Seyfert nuclei, in order to correct for the transmission of the Earth's atmosphere and to provide flux calibration. The L-band magnitudes of the standard stars were estimated from their V-band ($\lambda = 0.6$ μm) magnitudes, where we adopted the $V - L$ colors appropriate to the stellar types of individual standard stars (Tokunaga 2000).

Standard data analysis procedures were employed, using IRAF.[6] Initially, frames taken with an A (or B) beam were subtracted from frames subsequently taken with a B (or A) beam, and the resulting subtracted frames were added and divided by a spectroscopic flat image. Next, bad pixels and pixels hit by cosmic rays were replaced with the interpolated values of the surrounding pixels. Finally, the spectra of the Seyfert nuclei and the standard stars were extracted by integrating signals over 1.8″–2.2″, depending on the actual signal profiles. Wavelength calibration was performed by accounting for the wavelength-dependent transmission of the Earth's atmosphere. The spectra of the Seyfert nuclei were divided by the observed spectra of the standard stars, which were multiplied by the spectra of blackbodies with temperatures appropriate to the individual standard stars (Table 1). Flux calibration was done on the basis of the signals of the Seyfert galaxies and the standard stars detected inside our slit spectra. To reduce the scatter of the data points, appropriate spectral binning is employed, depending on the continuum flux levels of the final spectra.

[6] IRAF is distributed by the National Optical Astronomy Observatory, which is operated by the Association of Universities for Research in Astronomy (AURA), Inc., under cooperative agreement with the National Science Foundation.

REFERENCES

Barnes, J. E., & Hernquist, L. 1992, ARA&A, 30, 705
Barnes, J. E., & Hernquist, L. E. 1991, ApJ, 370, L65
Barth, A. J., Ho, L. C., Filippenko, A. V., & Sargent, W. L. 1995, AJ, 110, 1009
Benedict, G. F., Smith, B. J., & Kenney, J. D. P. 1996, AJ, 112, 1318
Bian, W., & Gu, Q. 2007, ApJ, 657, 159
Buta, R., Purcell, G. B., & Crocker, D. A. 1995, AJ, 110, 1588
Davies, R., Mueller Sánchez, F., Genzel, R., Tacconi, L., Hicks, E., Friedrich, S., & Sternberg, A. 2007, ApJ, 671, 1388
Efstathiou, A., Rowan-Robinson, M., & Siebenmorgen, R. 2000, MNRAS, 313, 734
Elmouttie, M., Koribalski, B., Gordon, S., Taylor, K., Houghton, S., Lavezzi, T., Haynes, R., & Jones, K. 1998, MNRAS, 297, 49
Feigelson, E. D., & Nelson, P. I. 1985, ApJ, 293, 192
Forbes, D. A., Norris, R. P., Williger, G. M., & Smith, R. C. 1994, AJ, 107, 984
Fukuda, H., Habe, A., & Wada, K. 2000, ApJ, 529, 109
Fukuda, H., Wada, K., & Habe, A. 1998, MNRAS, 295, 463
Fukue, J., Umemura, M., & Mineshige, S. 1997, PASJ, 49, 673
Gorjian, V., Werner, M. W., Jarrett, T. H., Cole, D. M., & Ressler, M. E. 2004, ApJ, 605, 156
Hernquist, L. 1989, Nature, 340, 687
Houck, J. R., et al. 2004, ApJS, 154, 18
Huchra, J., & Burg, R. 1992, ApJ, 393, 90
Imanishi, M. 2002, ApJ, 569, 44
———. 2003, ApJ, 599, 918
Imanishi, M., & Alonso-Herrero, A. 2004, ApJ, 614, 122
Imanishi, M., Dudley, C. C., Maiolino, R., Maloney, P. R., Nakagawa, T., & Risaliti, G. 2007, ApJS, 171, 72
Imanishi, M., Dudley, C. C., & Maloney, P. R. 2006, ApJ, 637, 114
Imanishi, M., & Wada, K. 2004, ApJ, 617, 214
Isobe, T., Feigelson, E. D., & Nelson, P. I. 1986, ApJ, 306, 490
Kaspi, S., Smith, P. S., Netzer, H., Maoz, D., Jannuzi, B. T., & Giveon, U. 2000, ApJ, 533, 631
Kawakatu, N., Imanishi, M., & Nagao, T. 2007, ApJ, 661, 660
Kawakatu, N., & Umemura, M. 2002, MNRAS, 329, 572
Knapen, J. H. 2005, A&A, 429, 141
Knapen, J. H., Beckman, J. E., Heller, C. H., Shlosman, I., & de Jong, R. S. 1995, ApJ, 454, 623
Knapen, J. H., Pérez-Ramírez, D., & Laine, S. 2002, MNRAS, 337, 808
Leitherer, C., Vacca, W. D., Conti, P. S., Filippenko, A. V., Robert, C., & Sargent, W. L. W. 1996, ApJ, 465, 717
Lutz, D., et al. 1996, A&A, 315, L269
Maciejewski, W., Teuben, P. J., Sparke, L. S., & Stone, J. M. 2002, MNRAS, 329, 502
Makino, J. 1997, ApJ, 478, 58
Maoz, D., Barth, A. J., Sternberg, A., Filippenko, A. V., Ho, L. C., Macchetto, F. D., Rix, H.-W., & Schneider, D. P. 1996, AJ, 111, 2248
Marconi, A., Moorwood, A. F. M., Origlia, L., & Oliva, E. 1994, Messenger, 78, 20
Matsushita, S., Kawabe, R., Kohno, K., Matsumoto, H., Tsuru, T. G., & Vila-Vilaró, B. 2005, ApJ, 618, 712
Mauder, W., Weigelt, G., Appenzeller, I., & Wagner, S. J. 1994, A&A, 285, 44
Mihos, J. C., & Hernquist, L. 1996, ApJ, 464, 641
Montenegro, L. E., Yuan, C., & Elmegreen, B. G. 1999, ApJ, 520, 592
Mouri, H., Kawara, K., Taniguchi, Y., & Nishida, M. 1990, ApJ, 356, L39
Noguchi, M. 1988, A&A, 203, 259
Norman, C. A., & Ikeuchi, S. 1989, ApJ, 345, 372
Ohsuga, K., & Umemura, M. 1999, ApJ, 521, L13
———. 2001, ApJ, 559, 157
Ohsuga, K., Umemura, M., Fukue, J., & Mineshige, S. 1999, PASJ, 51, 345
O'Neill, P. M., Nandra, K., Papadakis, I. E., & Turner, T. J. 2005, MNRAS, 358, 1405
Onodera, S., Koda, J., Sofue, Y., & Kohno, K. 2004, PASJ, 56, 439
Panessa, F., & Bassani, L. 2002, A&A, 394, 435
Panessa, F., Bassani, L., Cappi, M., Dadina, M., Barcons, X., Carrera, F. J., Ho, L. C., & Iwasawa, K. 2006, A&A, 455, 173
Peeters, E., Spoon, H. W. W., & Tielens, A. G. G. M. 2004, ApJ, 613, 986
Peterson, B. M., & Wandel, A. 1999, ApJ, 521, L95
Pogge, R. W. 1989, ApJ, 345, 730
Rayner, J. T., Toomey, D. W., Onaka, P. M., Denault, A. J., Stahlberger, W. E., Vacca, W. D., Cushing, M. C., & Wang, S. 2003, PASP, 115, 362
Rieke, G. H., & Lebofsky, M. J. 1985, ApJ, 288, 618
Rodríguez-Ardila, A., & Viegas, S. M. 2003, MNRAS, 340, L33
Rush, B., Malkan, M. A., & Spinoglio, L. 1993, ApJS, 89, 1
Saitoh, T. R., & Wada, K. 2004, ApJ, 615, L93
Shapiro, P. R., & Field, G. B. 1976, ApJ, 205, 762
Shinozaki, K., Miyaji, T., Ishisaki, Y., Ueda, Y., & Ogasaka, Y. 2006, AJ, 131, 2843
Shlosman, I., Begelman, M. C., & Frank, J. 1990, Nature, 345, 679
Siebenmorgen, R., Krugel, E., & Spoon, H. W. W. 2004, A&A, 414, 123
Soifer, B. T., Neugebauer, G., Matthews, K., Egami, E., & Weinberger, A. J. 2002, AJ, 124, 2980
Storchi-Bergmann, T., Wilson, A. S., & Baldwin, J. A. 1996, ApJ, 460, 252
Taniguchi, Y. 1999, ApJ, 524, 65
Thompson, T. A., Quataert, E., & Murray, N. 2005, ApJ, 630, 167
Tokunaga, A. T. 2000, in Allen's Astrophysical Quantities, ed. A. N. Cox (4th ed.; Berlin: Springer), 143
Tokunaga, A. T., Sellgren, K., Smith, R. G., Nagata, T., Sakata, A., & Nakada, Y. 1991, ApJ, 380, 452
Tomisaka, K., & Ikeuchi, S. 1986, PASJ, 38, 697
Toomre, A. 1964, ApJ, 139, 1217
Tremaine, S., et al. 2002, ApJ, 574, 740
Turner, T. J., George, I. M., Nandra, K., & Mushotzky, R. F. 1997, ApJS, 113, 23
Umemura, M., Fukue, J., & Mineshige, S. 1997, ApJ, 479, L97
———. 1998, MNRAS, 299, 1123
Voit, G. M. 1992, MNRAS, 258, 841
Wada, K., Meurer, G., & Norman, C. A. 2002, ApJ, 577, 197
Wada, K., & Norman, C. A. 1999, ApJ, 516, L13
———. 2001, ApJ, 547, 172
———. 2002, ApJ, 566, L21
Watabe, Y., & Umemura, M. 2005, ApJ, 618, 649
Werner, M. W., et al. 2004, ApJS, 154, 1
Wilson, A. S., Helfer, T. T., Haniff, C. A., & Ward, M. J. 1991, ApJ, 381, 79